Shear fracture mechanical properties and acoustic emission characteristics of discontinuous jointed granite

Gang WANG
Key Laboratory of Rock Mechanics and Geohazards of Zhejiang Province, Shaoxing University, Shaoxing, Zhejiang 312000, China

Lei-bo SONG
Key Laboratory of Rock Mechanics and Geohazards of Zhejiang Province, Shaoxing University, Shaoxing, Zhejiang 312000, China, song_leibo@163.com

Xi-qi LIU
School of Civil Engineering, Wuhan University, Wuhan, Hubei 430070, China

Chun-yan BAO
Key Laboratory of Rock Mechanics and Geohazards of Zhejiang Province, Shaoxing University, Shaoxing, Zhejiang 312000, China

See next page for additional authors

Custom Citation

Shear fracture mechanical properties and acoustic emission characteristics of discontinuous jointed granite

Authors

Gang WANG, Lei-bo SONG, Xi-qi LIU, Chun-yan BAO, Man-qing LIN, and Guang-jian LIU

Shear fracture mechanical properties and acoustic emission characteristics of discontinuous jointed granite

WANG Gang[1, 2, 3], SONG Lei-bo[1, 3], LIU Xi-qi[2], BAO Chun-yan[1, 3], LIN Man-qing[4], LIU Guang-jian[1, 3]

1. School of Civil Engineering, Shaoxing University, Shaoxing, Zhejiang 312000, China

2. School of Civil Engineering, Wuhan University, Wuhan, Hubei 430070, China

3. Key Laboratory of Rock Mechanics and Geohazards of Zhejiang Province, Shaoxing University, Shaoxing, Zhejiang 312000, China

4. School of Resources and Safety Engineering, Wuhan Institute of Technology, Wuhan, Hubei 430070, China

Abstract: To investigate the fracture mechanical behavior and failure mechanism of jointed rock mass under compression and shear load, shear tests were carried out on intact and discontinuous jointed granite. The macroscopic mechanical properties, acoustic emission signal characteristics and mesoscopic evolution law by particle flow simulation were analyzed through the experiment. A method predicting shear failure of granite was proposed by using the acoustic emission signal characteristics and its key information points. The results show that the rock integrity is damaged by the joint, and the shear modulus and peak shear strength of the rock are reduced. In addition, the existence of joints will affect the propagation path and failure mode of cracks, and the influence will be weakened with the increase of normal stress. The normal stress and joints have significant effects on the acoustic emission characteristic points. The slow growth of acoustic emission signal and the continuous decline of b value can be used as the precursor characteristics of rock shear failure. The acoustic emission signal characteristics and its key information points can be used to effectively predict the shear failure process of granite. The research results provide a reference for the shear failure mechanism analysis and stability prediction of jointed rock mass.

Keywords: rock mechanics; discontinuous joint; granite; acoustic emission; failure mechanism

1 Introduction

The jointed rock mass is a common kind of complex engineering medium in the tunnel, slope, underground powerhouse, and other projects. From the engineering point of view, it can be divided into the continuous and discontinuous jointed rock mass. For discontinuous jointed rock mass, after subjected to external loads, the rock mass mainly extends along the primary joints and the two ends of the rock bridge, forming a composite failure surface, whose mechanical characteristics and failure mechanism are complex. Therefore, the mechanical properties of discontinuous jointed rock mass are of great significance for the safety and stability of engineering and have always been a hot research issue[1−3].

The shear test is an important means to study the behavior of discontinuous jointed rock mass. It can well simulate the mechanical characteristics of the joint surface, and can fully reflect the propagation and coalescence characteristics of discontinuous joints under different normal stresses. Liu et al.[4] found that the dilatancy effect could make the rock bridge bear more compressive stress through the direct shear test, which leads to the enhancement of the shear strength of the rock bridge. Liu et al.[5−6] and Hu et al.[7] studied coplanar closed intermittent jointed rock mass to analyze the mechanical characteristics of discontinuous joints under direct shear stress and the evolution law of rock mass shear strength. Gehle et al.[8] made intermittent joint model specimens with different echelon arrangements and analyzed the mechanism of shear failure of intermittent joint rock mass based on the large deformation direct shear test. Zhang et al.[9] conducted the shear test on single joint rock samples and found that the joint width affected the failure mode of the rock mass. After the joint width changed to narrow, the specimen changed from large-scale tension-shear failure to shear failure mode. Lajtai[10] put forward the rock bridge failure theory that with the change of normal stress, the rock bridge failure is mainly divided into three failure modes: tension, shear, and extrusion. According to the above studies, the influence of joints on the mechanical behavior of rocks is preliminarily analyzed mainly from the perspective of the macroscopic failure characteristics of rocks.

In fact, rock instability is a process of gradual evolution from microfracture to macro failure, whose internal crystal dislocation and fracture will release stress waves to produce acoustic emission (AE). Therefore, acoustic emission

technology is an effective way to study the failure mechanism of rock mass[11−12]. Moradian et al.[13−14] compared the acoustic emission signal with the rock stress−strain curve and found that the acoustic emission ringing and energy characteristics can better reflect the activity of rock internal fracture events and the release of elastic strain energy. Zhao et al.[15] and Rudajev et al.[16] found that acoustic emission parameters can reflect the rock stress level and fracture stage, and the precursor characteristics of instability have obvious regularity. Cai et al.[17] identified the initiation time of the initial crack of the rock specimen through acoustic emission events and evaluated the damage degree of the rock. Xu et al.[18] and Chen et al.[19] carried out the shear test under different working conditions in the laboratory to explore the relationship between rock shear failure mode and acoustic emission characteristic parameters. Cheng et al.[20] took the intact sandstone as the research object and analyzed the evolution mechanism of sandstone shear cracking based on the acoustic emission system. Moradian et al.[21] carried out the shear test of jointed granite and discussed the acoustic emission count and energy characteristics during the shear fracture process of rock. On the whole, a large number of studies on the mechanical properties of the discontinuous jointed rock are carried out by some experts, which provides strong theoretical support and engineering guidance for the stability of jointed rock mass. However, it is not clear that the influence of the existence of joints on AE signals and failure precursor characteristics of rock shear fracture, so the internal relationship between the mechanical properties of macro shear fracture and microfracture of discontinuous jointed rocks remains to be further studied.

In view of this, shear tests of the discontinuous jointed granite are carried out in this study, and acoustic emission technology is used to monitor the whole process of fracture, and the influence of discontinuous coplanar joints on the mechanical properties and failure mode of granite are analyzed and the shear failure mechanism of discontinuous jointed granite is revealed based on acoustic emission characteristics, which provides a reference for the engineering design and construction of jointed rock mass.

2 Sample preparation

2.1 Physical and mechanical properties

The granite samples used in the test were derived from the underground powerhouse of Shuangjiangkou Hydropower Station on the Dadu River in Sichuan Province. The vertical buried depth of the powerhouse is about 320−500 m, and the in-situ stress is up to 20−30 MPa.

The surrounding rock of the powerhouse is porphyritic biotite potassium feldspar granite, and pegmatite veins are developed locally. The rock mass is dense and hard, and the structural planes in the rock mass are not developed, mostly in block or overall structure. Figure 1 shows the microstructure of the granite sample. Its mineral composition mainly includes quartz, potassium feldspar, and plagioclase. The accessory mineral is biotite. Additionally, it also contains a small amount of pyroxene, apatite, magnetite, and other components.
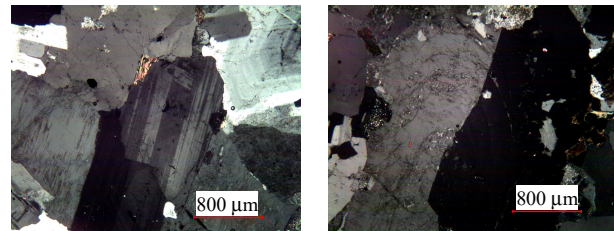

Fig. 1 Microstructure of granite sample

To ensure the reliability of the follow-up test, the density test and acoustic test were carried out on the granite sample, and the test results are shown in Fig.2. It can be seen from Fig.2 that the difference of density and the difference of longitudinal wave velocity between samples are less, and their distribution characteristics basically follow the normal distribution law. Further,
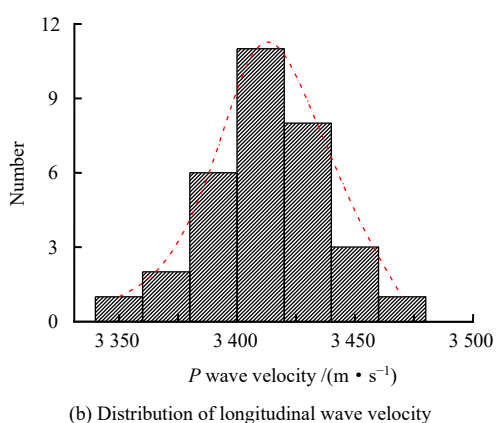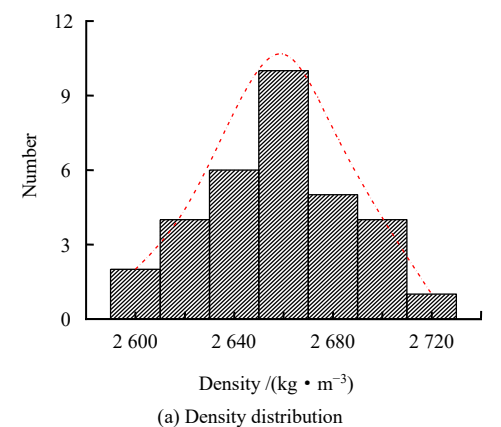

(a) Density distribution

(b) Distribution of longitudinal wave velocity

Fig. 2 Reliability testing of granite specimens

the Brazil splitting test and the uniaxial test were carried out to determine the mechanical properties of granite samples. The stress−strain curve and failure characteristics were drawn in Fig.3. The basic physical and mechanical properties are shown in Table 1. Good consistency can observed in the stress−strain curves of granite samples, and also in the failure characteristics. From the above analysis, it can be seen that the internal structure and physical and mechanical properties of the selected granite are less discrete, implying the test has high reliability.
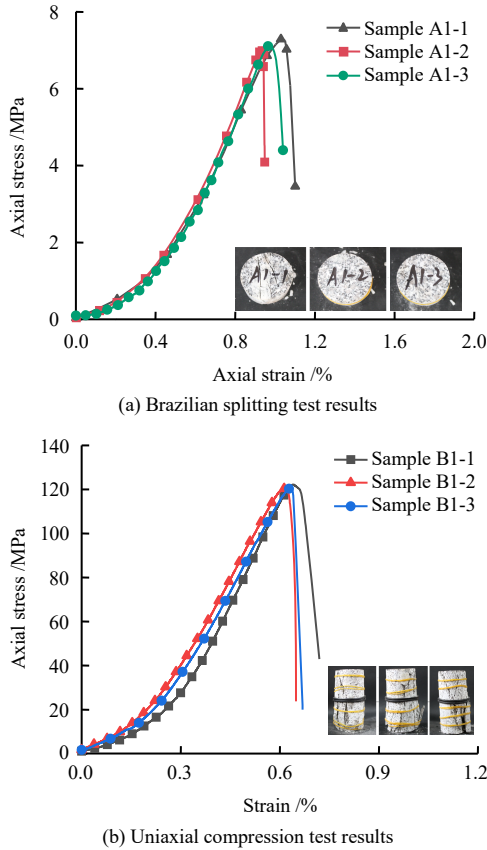

(a) Brazilian splitting test results

(b) Uniaxial compression test results

**Fig. 3 Stress-strain curves and failure characteristics**

Table 1 Basic physical and mechanical parameters of granite

Density /(g · cm⁻³)	Longitudinal wave velocity /(km · s⁻¹)	Elasticity modulus /GPa	Poisson's ratio	UCS (Uniaxial compressive strength) /MPa	Uniaxial tensile strength /MPa
2.60~2.72	3.35~3.50	33.8	0.21	120.71	8.26

2.2 Sample preparation and test scheme

The granite samples with discontinuous joints are made by wire cutting technology. First, the granite samples obtained from the underground powerhouse of Shuangjiangkou Hydropower Station are processed into 100 mm×100 mm×100 mm cubic samples, the flatness, parallelism, and perpendicularity of which must meet the standard requirements of the international rock mechanics test[22]. And then, the cubic sample is set on the machine tool of the cutting machine, and the wire cutting technology is used to make coplanar straight

joints with a length of 20 mm and a width of 0.4 mm at both ends along the middle of the sample. The spatial structure characteristics of the joint are shown in Fig.4(a) and the jointed granite sample is shown in Fig.4(b). In addition, a batch of 100 mm×100 mm×100 mm complete cubic granite specimens is used for the comparative analysis.
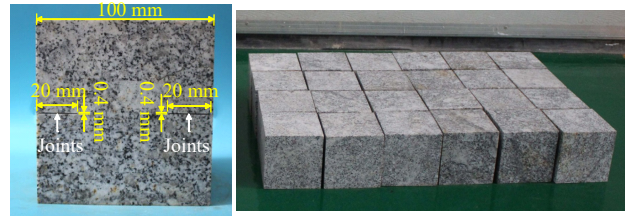
(a) Structural characteristics of joints   (b) Jointed granite sample

Fig. 4 Granite samples with discontinuous joints

The direct shear test of the granite sample is completed on the shear test system shown in Fig.5. The shear system is a microcomputer-controlled electrical stress direct shear instrument, which is composed of the loading system, hydraulic system, and computer operating system. The maximum normal load is 1 000 kN and the maximum horizontal load is 1 000 kN. In addition, the acoustic emission monitoring system shown in Fig.5 is used to monitor the behavior of granite samples during the whole shear process. The PAC full information acoustic emission signal analyzer is used in the acoustic emission monitoring system. The acquisition device has A/D converters with 8 channels and 16 channels, which can provide multiple sampling rates of 100, 500 kHz, as well as 3, 5, 10 MHz.
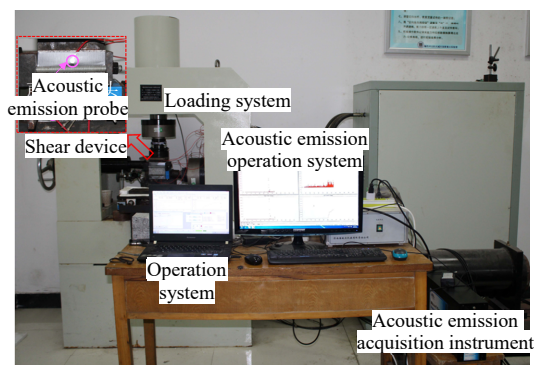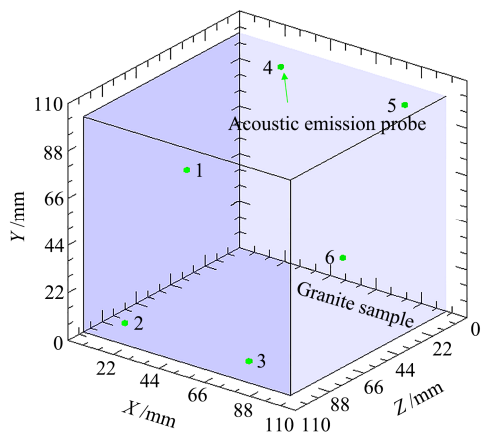

Fig. 5 Test system

The intact granite sample and the granite sample with discontinuous joints are subjected to the shear test under the conventional normal stress, and the normal stress is 5, 10, 15, and 20 MPa. The test process is mainly divided into two stages (shown in Table 2): (1) apply the normal load to the predetermined value at a loading speed of 0.5 kN · s⁻¹ by the loading control method; (2) the shear loading of horizontal displacement is carried out at a loading
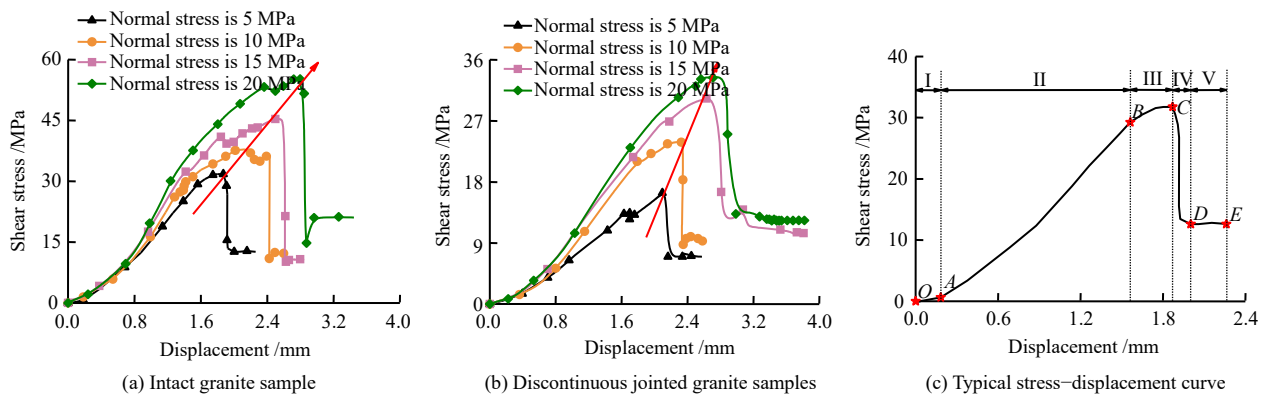
speed of 0.18 mm · min^{-1} by the displacement control method. When the test reaches the residual strength value, the test should be stopped. Before the test, the acoustic emission probes are placed on the rock sample. The layout scheme of the acoustic emission probes is shown in Fig.6. The acoustic emission monitoring system is synchronously operated and monitored during the shear process. In addition, the whole test process is recorded by the camera to analyze the failure evolution law of the sample. To ensure the accuracy of the test results, the tests are repeated three times on the granite under each normal stress.

Table 2   Test scheme

Specimen type	1st stage: normal loading			2nd stage: horizontal shear	
	Control mode	Normal static load /kN	Loading speed /(kN · s^{-1})	Control mode	Loading rate /(mm · min^{-1})
Intact granite / Discontinuous jointed granite	Force	50 100 150 200	0.5	Displacement	0.18

Fig. 6   Acoustic emission probe layout scheme

3   Shear failure characteristics

3.1 Deformation and strength

The stress−displacement curves of intact granite samples and discontinuous jointed granite samples are shown in Fig.7. The test curves of the two granite samples have certain similarities in Fig.7(a) and Fig.7(b). According to the morphological changes of the stress−displacement curve, it can be generalized into five stages as Fig.7(c) shows.

Initial slow growth stage I (*OA*): At the initial stage of shear loading, the stress−displacement curve of the sample shows an upward shape, that is, with the increase of shear displacement, the growth rate of shear stress gradually increases and tends to be stable at point *A*. There are two main reasons for this, on the one hand, the micro-cracks in the specimen are closed under the action of shear force; on the other hand, there is a gap between the specimen and the shear box, which is close to each other under the action of shear force in the early stage of shear action.

Linear elastic deformation stage II (*AB*): the stress−displacement curve of the specimen at this stage is approximately linear, that is, the shear stress increases linearly or approximately linearly with the increase of shear displacement.

Unstable fracture development stage III (*BC*): with the increase of shear displacement, the growth rate of shear stress gradually slows down, and the stress−displacement curve changes from approximately linear type to upper convex type, that is, point *B* is the inflection

(a) Intact granite sample   (b) Discontinuous jointed granite samples   (c) Typical stress−displacement curve

Fig. 7   Stress−displacement curves of granite specimen

point from elasticity to plasticity, and the rock reaches the maximum bearing capacity at point *C*. In this process, the development of microcracks in the rock changes qualitatively, and the fracture occurs continuously until the specimen is destroyed.

Post peak fracture stage IV (*CD*): after the shear stress reaches the peak, it drops rapidly with the increase of

shear displacement, and the sample shows strong brittle characteristics. The main reason for the rapid drop of bearing capacity is the rapid coalescence of macro cracks in the sample at this stage.

Residual strength stage V (*DE*): in this stage, the stress−displacement curve of the sample is relatively smooth. Under the joint action of normal stress and

horizontal shear stress, the upper and lower fracture specimens slide relatively to each other, and the friction of the rough fracture surface makes the fracture specimens still maintain a certain residual strength.

Through further analysis of Figs .7(a) and 7(b), it can be found that the strength and deformation characteristics of intact granite samples and discontinuous jointed granite samples are closely related to their normal stress. The peak shear strength and the peak shear displacement of both specimens increase with the increase of normal stress. However, due to the existence of discontinuous joints, the strength and deformation characteristics of the two

samples show some differences under the same normal stress. For example, under a 5 MPa normal stress, the average peak shear strength of intact granite is 31.8 MPa, and the peak shear displacement is 1.87 mm. The average shear strength of granite with discontinuous joints is 16.4 MPa and the peak shear displacement is 2.09 mm. To analyze the influence of discontinuous joints on the strength and deformation characteristics of the granite, the shear stiffness, peak shear strength, and peak shear displacement of the two samples are further statistically analyzed, and the statistical results are drawn in Fig.8. The following laws can be found in Fig.8:

| (a) Shear stiffness | (b) Peak shear strength | (c) Peak shear displacement |
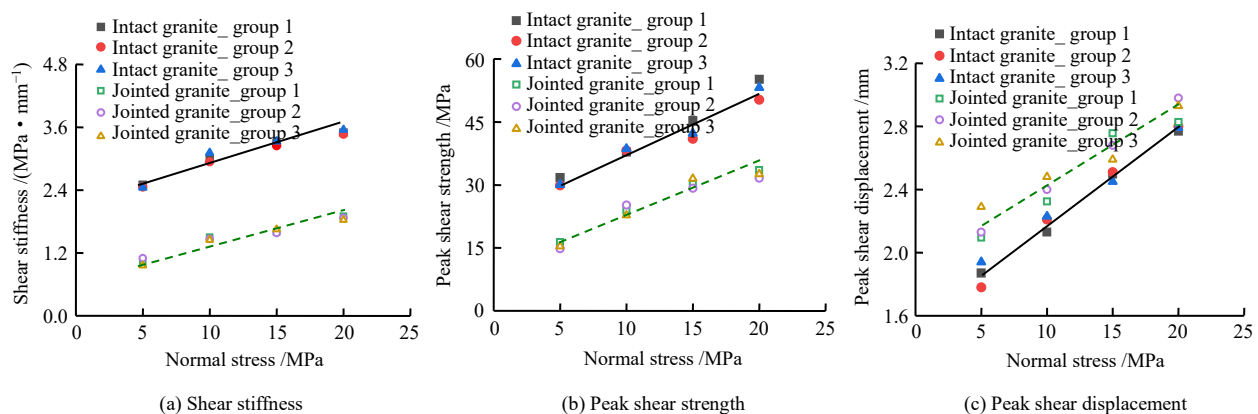
**Fig. 8 Influence of discontinuous joints on deformation and strength characteristics of granite**

(1) The shear stiffness, peak shear strength, and peak shear displacement all increase with the increase of normal stress, that is, the increase of normal stress enhances the ability of the rock to resist shear failure.

(2) Compared with the intact granite sample, the existence of discontinuous joints weakens the shear stiffness of the rock, reduces its peak shear strength, and boosts its peak shear displacement.

3.2 Failure characteristics

The failure mode of the specimen is the macroscopic behavior of the rock with the comprehensive mechanical effect. Figure 9 shows the shear fracture surface of a typical discontinuous jointed granite. In the shear process, because the upper and lower joints of the shear plane dislocate relatively, a certain depth of tensile groove appears at the end of the rock bridge under tension and there is obvious milky white powder on the failure surface, which is the wear powder area formed by crushing and shearing of feldspar and cementitious materials in granite. Due to the random distribution of a certain number of biotite particles in the hard quartz, a certain length of black scratches are formed along the movement direction during the shear sliding process, the part of which is excessively flat, and the shear surface wear is small, and only a small amount of debris appears, forming an obvious hard shear

sliding zone. Table 3 further summarizes the fracture section morphology figures of intact granite and jointed granite samples under different normal stress conditions. It can be seen from Table 3 that the roughness of the intact granite shear surface is larger, forming an obvious fluvial fracture morphology, and its trend is consistent with the loading direction. In addition, there are a few tensile grooves around the fluvial bulge. With the increase of normal stress, the shear fracture surface of the two granite types tends to be severe worn, the cross-section gradually changes from different sizes of debris to rock powder, the shear surface tends to be flat, and the cross-section roughness gradually decreases, and the specimen finally
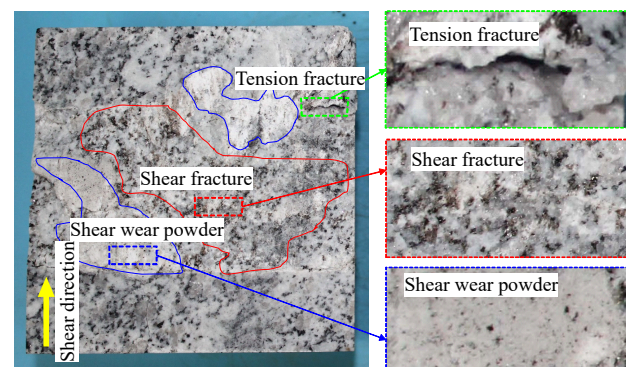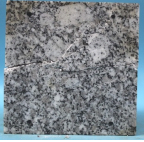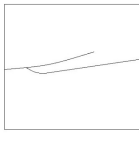

Fig. 9 Typical failure mode of granite
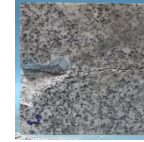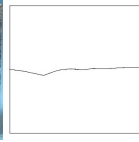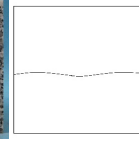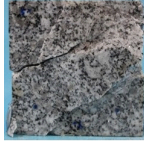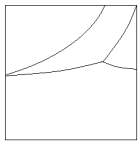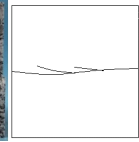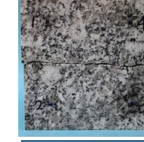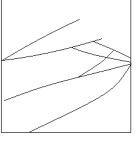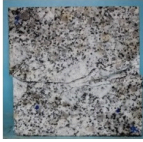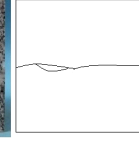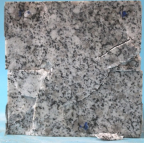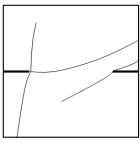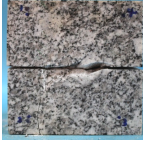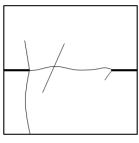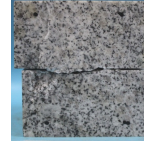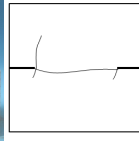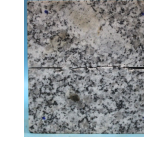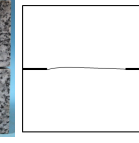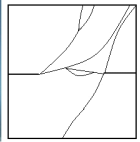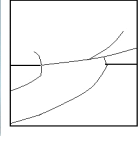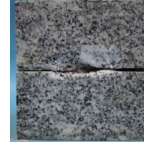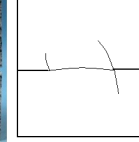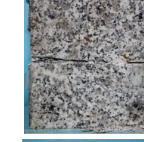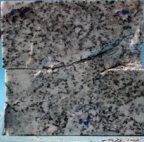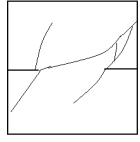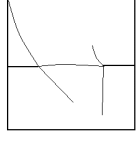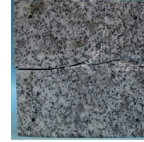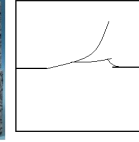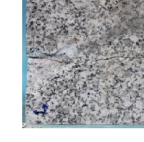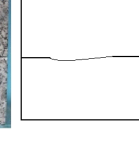
changes from tensile shear composite failure to shear failure.

Table 3 also summarizes the crack morphology figures of intact granite samples and discontinuous jointed granite samples. By the comparison, it can be found that the crack morphology and number of the sample are affected by the normal stress and discontinuous joints, and the specific laws are as follows:

Table 3   Failure characteristics of granite

Type	Normal stress 5 MPa		Normal stress 10 MPa		Normal stress 15 MPa		Normal stress 20 MPa	
	Crack morphology	Crack sketch	Crack morphology	Crack sketch	Crack morphology	Crack sketch	Crack morphology	Crack sketch
Intact granite								
Discontinuous jointed granite								

(1) For the intact granite samples, the crack starts at the middle position on both sides of the specimen, which is caused by the stress concentration created by the shear loading, forming a macro oblique crack at a certain angle to the horizontal direction. With the increase of normal stress, the angle of oblique crack decreases gradually, the specimen changes from tension shear composite failure to single shear failure mode, and the number of cracks decreases synchronously.

(2) For the discontinuous jointed granites, the macroscopic cracks often begin at the joint ends because of the significant stress concentration at the joint ends during the loading process. At this moment, the crack mainly propagates along the primary joints and both ends of the rock bridge under the combined action of compression and shear, forming continuous shear cracks and a certain number of vertical tensile cracks accompanied. With the increase of normal stress, the propagation of secondary cracks is greatly restrained, the vertical cracks become shorter and even disappear, and the total number of cracks tends to decrease. The specimen changes from tensile shear composite failure to single shear failure.

4   Shear failure mechanism

4.1 Analysis of shear failure mechanism

The acoustic emission monitoring system collects the ringing characteristics, energy characteristics, and b value characteristics of granite samples, and these signal characteristics can provide strong support for analyzing the evolution characteristics of internal damage. Specifically, the ringing characteristics of acoustic emission can reflect

the activity of rock internal fracture events and the cumulative damage degree of rock. The energy characteristics can characterize the elastic strain energy released by the crack propagation in the rock and reflect the strength of rock fracture. The energy E of a single acoustic emission signal is defined as[23−24]

$$E = \frac{1}{R} \int_{t_i}^{t_j} U^2(t)\, \mathrm{d}t \qquad (1)$$

where t_i and t_j are the time when the acoustic emission signal wave exceeds the threshold at the first time and falls below the threshold again; R value is the internal resistance parameter of acoustic emission acquisition equipment; and U is the voltage difference.

The characteristics of the b value are associated to the incubation, development, upheaval, and other evolution of rock fracture events, and it reflects the failure process of rocks to a certain extent. The calculation formula of b value[25−26] is

$$\lg N = a - b \frac{A_{dB}}{20} \qquad (2)$$

$$A_{dB} = 20 \lg A_{max} \qquad (3)$$

where A_{max} is the maximum amplitude of acoustic emission impact expressed in microvolts; A_{dB} is the maximum amplitude of acoustic emission expressed in decibels; N is the number of acoustic emission events with the

amplitude greater than or equal to A_{dB}; a is an empirical constant; and b is the b value of acoustic emission.

The location of the rock internal failure can be determined by the emission location map, and the macro crack propagation process can be observed with the help of the sample failure synchronously recorded by the camera.

In addition, to analyze the deterioration process of rock structure from the mesoscopic point of view, a particle flow aggregate in a rectangular area of 100 mm×100 mm is established by using the PBM (parallel bond model) contact model in PFC software, where the particle radius is set within the range of 0.31−0.51 mm and the particle porosity is 0.14. 10 922 particles are randomly generated, and the particle size is subject to the uniform distribution. During the test, a normal stress is applied to the upper shear box, and a same horizontal shear rate is given on the restraint plate of the upper shear box (see Fig.10(a)). The mesoscopic parameters of the model finally determined by using the trial and error method are shown in Table 1. The comparison results of numerical test and laboratory test under normal stress of 5 MPa are shown in Fig.10(b), the evolution laws of the stress−displacement curve of which are basically consistent. A macro shear fracture zone is formed in the middle of the rock specimen, and multi-level cross microcracks are derived around the macro main crack, failure modes of which are similar. Further,

(a) Numerical model of intact specimen

(b) Comparison diagram of numerical test and shear test of the intact specimen under 5 MPa

(c) Numerical model of joint specimen

(d) Comparison diagram of numerical test and shear test of the joint sample under 5 MPa
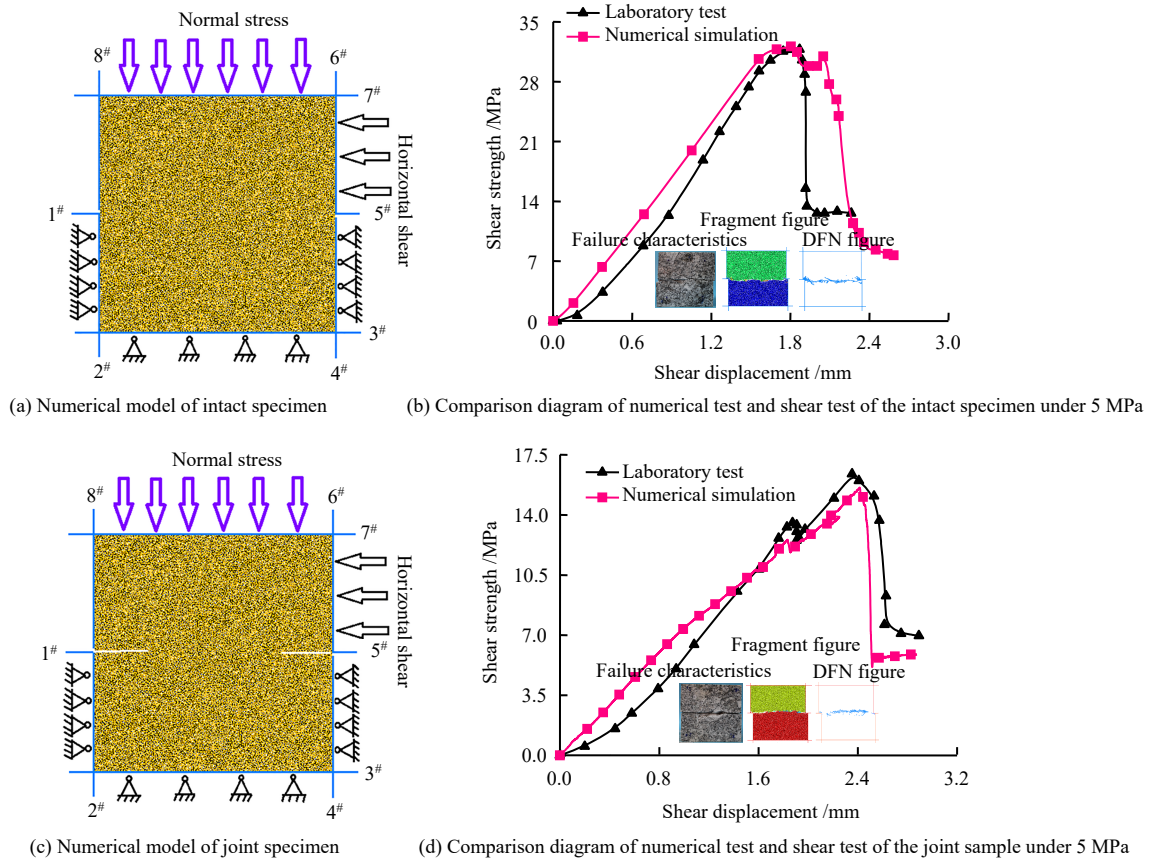
Fig. 10 PFC numerical simulation

rock joints are simulated by deleting particles with a certain thickness at a specific location, the thickness and the length of which are 0.4 mm and 20 mm. The location and geometric shape of joints are consistent with the discontinuous jointed granite specimens used in the laboratory test (see Fig.10(c)). The comparison between the numerical test and the laboratory test under the normal stress of 5 MPa is shown in Fig.10(d), the evolution laws of the stress−displacement curves of which are basically consistent. Under the action of stress concentration, the joint tip of the rock specimen cracks, and finally forms a shear core on the rock bridge. There is a certain amount of rock debris on the fracture surface. The failure modes of the two types of tests are similar. According to the above analysis, the macro mechanical parameters and fracture morphology of the granite particle flow model are basically consistent with the laboratory test results, so the corresponding numerical simulation can be carried out by using this particle flow model.

Figure 11 summarizes the test results under 5 MPa normal stress, including the test curve, acoustic emission characteristic signal curve, failure evolution characteristics, and numerical simulation contact force evolution process of jointed granite. According to the comparative analysis, the failure characteristics of jointed granite can be better reflected by the evolution characteristics of acoustic emission. The specific laws are as follows:

(1) When the jointed granite is in the initial slow growth stage I and linear elastic deformation stage II, the acoustic emission ringing count rate and energy are maintained at a low level, and the cumulative ringing count and cumulative energy are in a quiet period. The b value in the two stages is at a high value in general. Although it fluctuates slightly, it is basically maintained at the level of 0.148 0−0.159 3. From the positioning results, it can be seen that there are only a few acoustic emission events near the joint end, and the number of micro-fractures is small in general (see Fig.11(b)), which is consistent with the stress concentration phenomenon at the joint end in Fig.11(d) numerical simulation. In combination with Fig.11(c), it can be observed that there is no obvious macro crack on the sample surface during this process, and only the closure joints can be observed. This indicates that there is less damage to the granite in the two stages. Although a small number of microcracks will be initiated in the sample, accompanied by the release of a small amount of elastic energy, the crack propagation activity is relatively small, small-scale crack development is dominant, and the whole is in the process of gradual and stable propagation.

(2) When the jointed granite enters the unstable

fracture development stage III, the acoustic emission ringing count rate and energy show an increasing trend with the increase of shear stress, but the increased range is small on the whole, and the cumulative ringing count and cumulative energy are in a slow rising period. In this stage, the b value shows a continuous downward trend. As shown in Fig.11(d), the tensile and compressive stress concentration tends to be obvious at the upper and lower ends of the joint, and the particle contact force increases (the force chain coarsens), resulting in an increase in the number of acoustic emission events at the ends of the two joints and the area between them (seen in Fig.11(b)), which can macroscopically represent the occurrence of a small number of macro cracks at the ends of the joint shown in Fig.11(c). It indicates that with the increase of shear displacement, the internal damage of granite is accumulating, accompanied by stress release and energy dissipation, resulting in the continuous initiation and propagation of internal cracks in the rock from small-scale fracture to large-scale fracture. The rock is in the development stage of unstable fracture on the whole.

(3) When the jointed granite enters the post-peak fracture stage IV, the jointed granite sample changes from the subcritical stable state to the unstable state, the acoustic emission ringing count rate and energy increase sharply, and then show the fluctuation characteristics of order of magnitude difference, the cumulative ringing count and cumulative energy synchronously show step increase and the acoustic emission ringing and energy turn into a sharp rise period. In this stage, the b value drops rapidly to 0.095 6. From the positioning results, it can be seen that the number of acoustic emission events at the ends of the two joints and the area between them increased sharply, forming a macro fracture zone (seen in Fig.11(b)). At this moment, under the combined action of tension and compression shear (seen in Fig.11(d)), contact forces of a large number of particles at the end of joints can exceed the cohesive strength, and the contact force chain breaks, resulting in the rapid propagation of micro-cracks in the sample and the appearance of macro main cracks (seen in Fig.11(c)). At this stage, the proportion of small-scale fracture in the rock decreases, the proportion of large-scale fracture increases, and the cracks propagate, overlap, and coalesce rapidly, resulting in large-scale fracture events with high energy, and finally the main fracture cracks are formed. It should be noted that the ringing count rate and energy of jointed granite before and after the peak point show certain fluctuation characteristics, because after entering the unstable propagation stage, the dynamic cyclic action of stress concentration→ crack propagation → stress release occurs at the crack

tip, which makes the crack propagation show the characteristics of intermittent growth.

(4) When the jointed granite enters the residual strength stage V, the acoustic emission ringing count rate and energy return to a low level again. Although the cumulative ringing count and cumulative energy are still increasing, their increase rate is significantly reduced, and the acoustic emission ringing and energy are in a low-speed growth period. From the positioning results, it can be seen that a large number of fracture events emerge in the rock bridge

section, and oblique fracture zones are generated at a small angle with the horizontal along the joint ends (seen in Fig.11(b)). From Fig.11(c), it can be observed that both ends of the joint are penetrated by the macro cracks. In Fig.11(d), the contact force changes from the previous ordered deflection mode to the current disordered "point to point" contact mode, which confirms the generation of cross-section slip movement. In this stage, the damage of granite is less and the energy released is low. On the whole, the rock is in a stable sliding wear stage.

(a) Characteristic comparison diagram of test curve and acoustic emission energy, ringing and *b* value

(b) Acoustic emission positioning results （Unit: mm）

(c) Macroscopic crack growth process

(d) Evolution process of micro contact force

Fig. 11 Comparison of test curve, acoustic emission characteristics, and failure characteristics of jointed granite under 5 MPa normal stress

(a) Characteristic comparison diagram of test curve and acoustic emission energy, ringing and *b* value

(b) Acoustic emission positioning results （Unit： mm）

(c) Macroscopic crack growth process
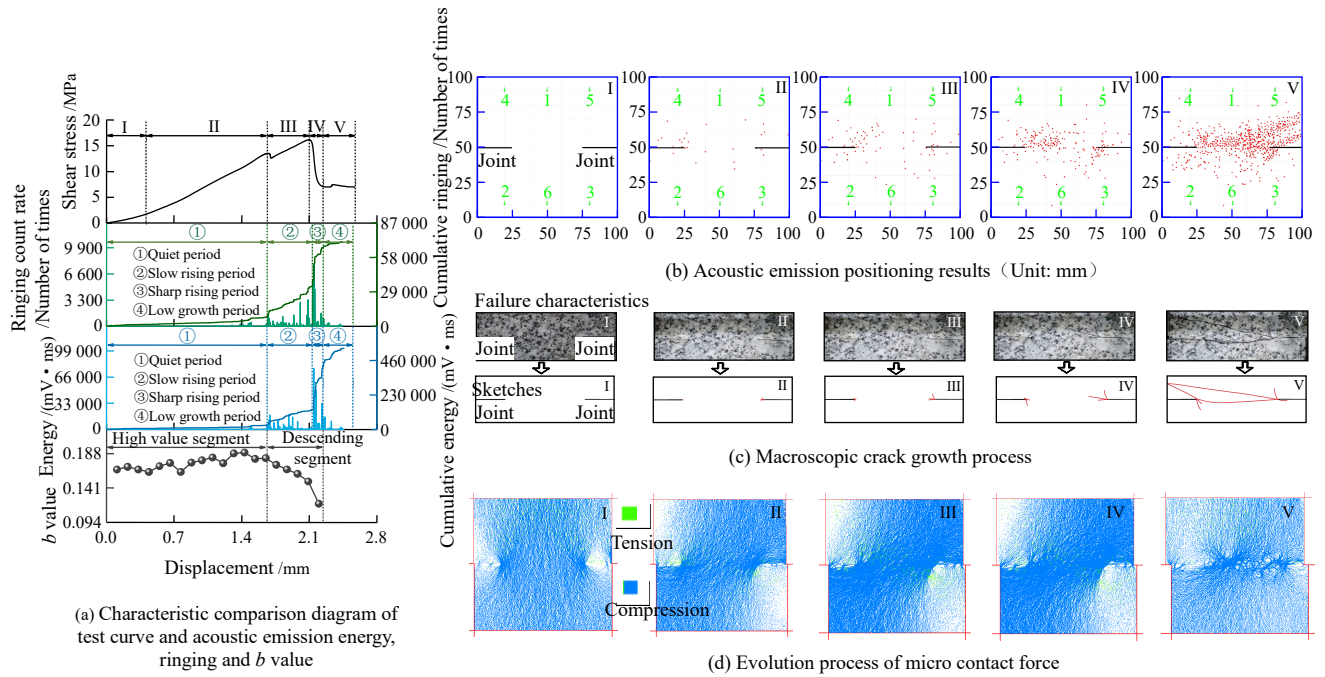
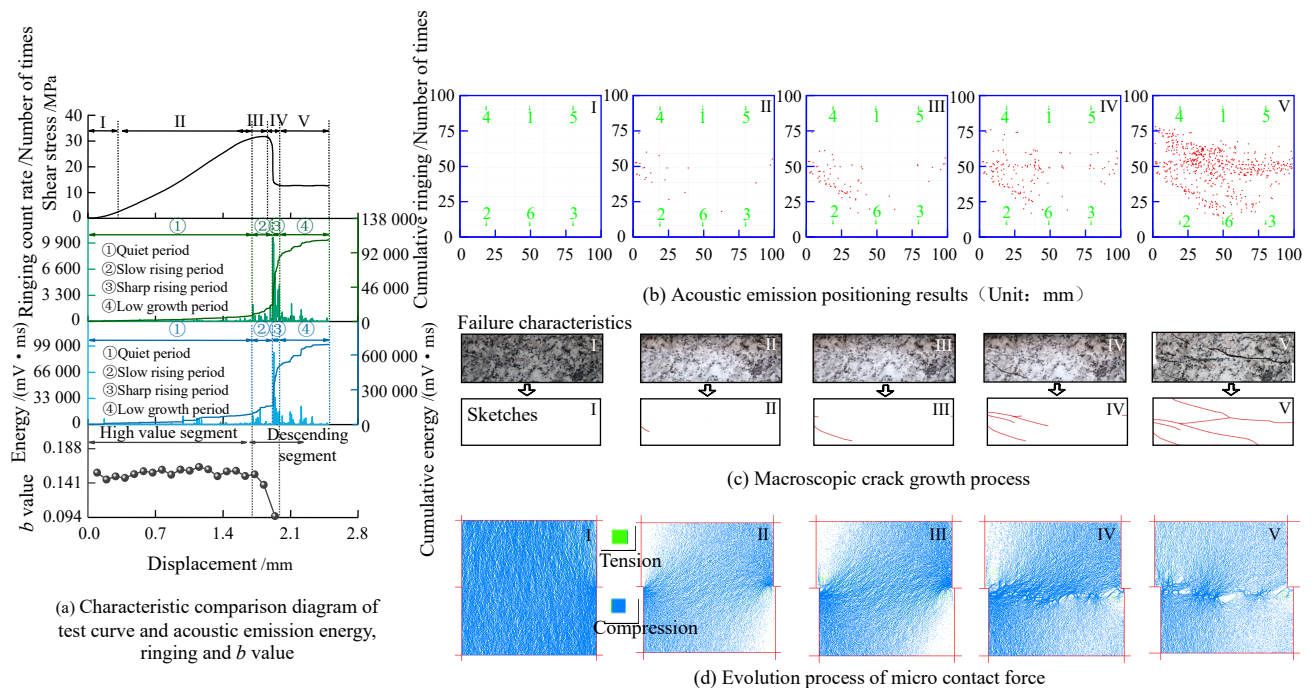(d) Evolution process of micro contact force

Fig. 12 Comparison of test curve, acoustic emission characteristics, and failure characteristics of intact granite under 5 MPa normal stress

Figure 12 presents the test curve, acoustic emission characteristic signal curve, failure characteristic evolution process, and numerical simulation contact force evolution process of intact granite under 5 MPa normal stress. From the comparison of Figs. 11 and 12, it can be seen that, for jointed granite, the crack initiates at the middle of both sides of the specimen due to the stress concentration caused by shear loading. Although the deformation characteristics and acoustic emission characteristics of the both have some differences in magnitude, their processes present similar evolution laws. Therefore, according to the above analysis, the changing trend of acoustic emission characteristic signal and its key point information can be used to predict the internal deformation and failure state of rock. Specifically, when the acoustic emission ring count rate and energy are kept at a low level, and the acoustic emission b value is at a high value, the rock is often in the initial slow growth stage or linear elastic deformation stage. When the b value reaches the starting point of continuous decline segment, it indicates that the rock has begun to enter the stage of unstable fracture development, and the system has entered the subcritical stable state. When the cumulative ringing count and cumulative energy increase sharply, it indicates that the rock changes from subcritical stable state to an unstable state and the rock enters the post-peak fracture stage. When the acoustic emission ringing count rate and energy are at a low level again, and the increase rate of cumulative ringing count and cumulative energy slows down, which indicates that the rock is in the residual strength stage.

4.2 Influence of normal stress and joints on acoustic emission signal characteristics

The above analysis suggests that the deformation and failure state of rock under shear load can be judged by using acoustic emission characteristic signals. There are several key points in this method that need to be paid attention to, that is, the initiation point of the sudden increase of the cumulative ringing count, the initiation point of the sudden increase of the cumulative energy, and the initiation point of the declining segment of the b value, which is an important basis for judging the state of the rock, so these are further analyzed in detail.

Figure 13 summarizes the test curves of acoustic emission cumulative ringing count, cumulative energy, and b value of intact granite and jointed granite under different normal stresses. The following laws can be found in the comparison and analysis of Fig.13:

(1) No matter what normal stress the granite is under or whether it contains joints, the characteristics of acoustic emission cumulative ringing count and cumulative energy

can be divided into quiet period, slow rising period, sharp rising period, and low-speed growth period as shown in Figs. 11(a) and 12(a). In addition, the b values of acoustic emission are both in the high magnitude segment and the declining segment with obvious segment characteristics. This shows that the deformation and failure characteristics of rocks can be predicted by using acoustic emission signals, which has certain universality.

(2) The displacement at the initiation point of cumulative ringing count sudden increase, the displacement at the initiation point of cumulative energy sudden increase, and the displacement at the initiation point of the declining segment of b value in intact granite and jointed granite all increase as the normal stress increases. This implies that with the increase of normal stress, the propagation of internal cracks in rock will be limited to a certain extent, the rock is less prone to fracture failure, the release of energy is also delayed, and the failure time from microcrack to large crack is also delayed correspondingly.

Through further observation and comparison of Figs. 13(a)−13(c) and 13(d)−13(f), it can be found that there are certain differences in acoustic emission characteristics and quantities of key points between intact granite and jointed granite. For this purpose, the statistics of this difference are shown in Fig.14. From the results, it can be seen that under the same normal stress, the displacement at the initiation point of the sudden increase of the ringing count and the displacement at the initiation point of the sudden increase of accumulated energy of jointed granite are almost higher than those of the intact granite, while the displacement at the initiation point of the declining segment of b value is lower than that of the intact granite, indicating that the existence of joints promotes the relatively earlier occurrence of large fracture events, the part elastic strain of rock energy will be released at this time, and then the coalescence of the internal crack will be delayed. In addition, Fig.14 also shows the maximum cumulative ring count, the maximum cumulative energy, and the lowest point of the b value of a group of granite samples. From the figure, it can be found that the normal stress has a positive correlation with the maximum cumulative ring count and the maximum cumulative energy of the two types of samples, which means that more energy is required to drive the rock to fracture with the increase of the normal stress. However, the lowest point of the b value decreases with the increase of normal stress, which indicates that the greater the normal stress is, the more intense the crack development changes during the shear process, and the greater its failure severity is. Under the same normal stress, the maximum cumulative

ring count and maximum cumulative energy of jointed granite are smaller than those of intact granite, and the lowest point of the *b* value is higher than that of intact granite, indicating that the crack energy required for the failure of jointed granite is less, which is also the reason why the joint rock mass in the project is more prone to failure. The key point information of acoustic emission signal in the granite during loading is seen in Table 4.
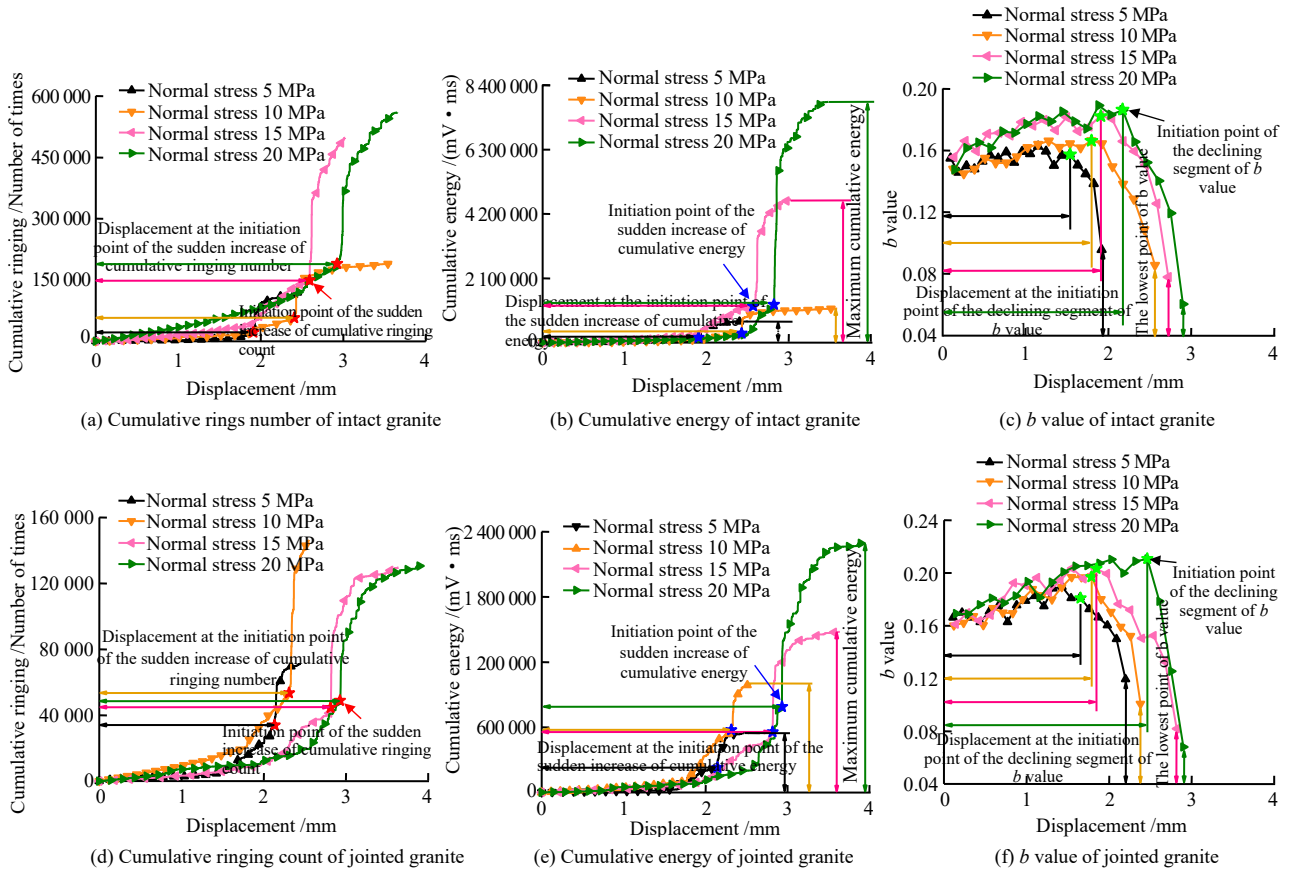

Fig. 13　Comparison of acoustic emission signals of intact granite and jointed granite under different normal stresses
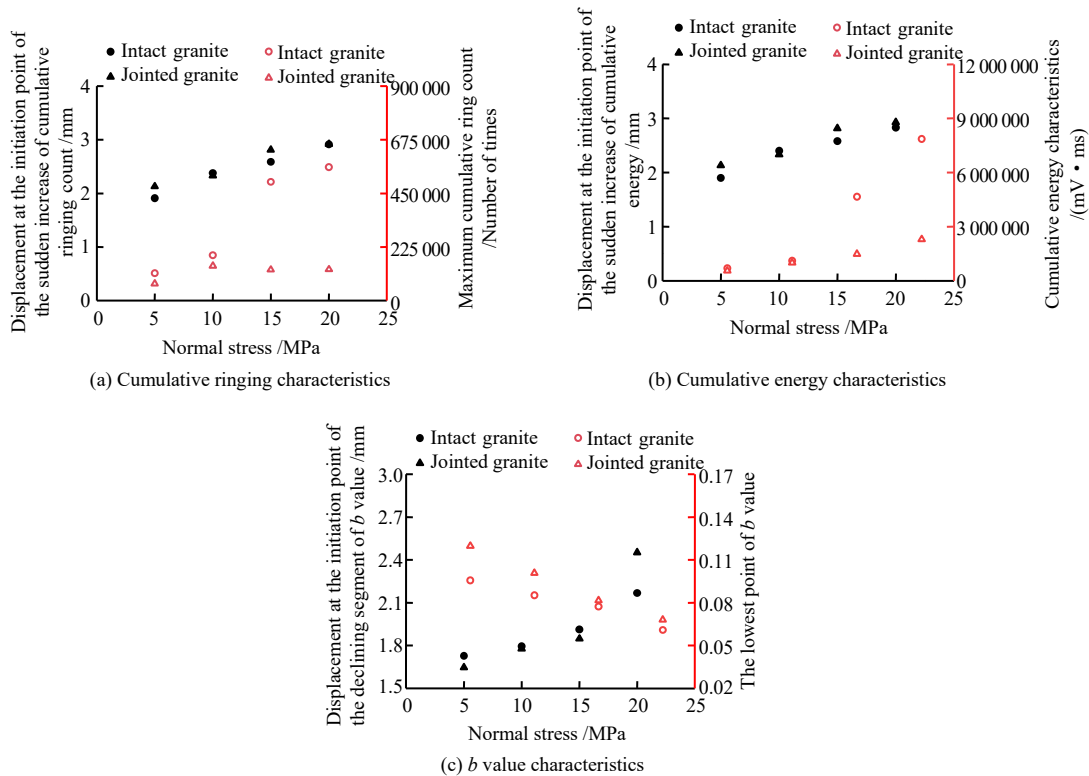

Fig. 14　Influence of normal stress and joint on key points of acoustic emission signal characteristics

Table 4   Key point information of AE signal

Sample type	σ_n /MPa	Key point	Cumulative ringing		Cumulative energy		b value	
			Displacement at the initiation point of sudden increase /mm	Maximum/ Number of times	Displacement at the initiation point of sudden increase /mm	Maximum /(mV · ms)	Displacement at the initiation point of declining segment /mm	The lowest point of the b value
Intact granite	5	1#	1.91	114 624	1.92	693 513	1.73	0.095 6
		2#	1.85	128 956	1.85	748 954	1.68	0.092 3
		3#	1.89	119 585	1.92	710 269	1.70	0.096 3
	10	1#	2.38	190 260	2.43	1 106 320	1.79	0.085 2
		2#	2.31	210 521	2.33	1 565 547	1.80	0.082 3
		3#	2.26	189 521	2.30	1 362 328	1.77	0.086 6
	15	1#	2.59	498 294	2.58	4 656 442	1.91	0.077 3
		2#	2.55	512 302	2.55	3 985 652	1.92	0.070 2
		3#	2.62	485 463	2.60	4 455 454	1.94	0.075 5
	20	1#	2.91	560 228	2.83	7 859 812	2.17	0.060 9
		2#	2.81	605 155	2.87	7 026 754	2.09	0.062 2
		3#	2.85	570 233	2.80	6 508 954	2.11	0.064 5
Jointed granite	5	1#	2.13	71 107	2.31	545 240	1.65	0.119 7
		2#	2.15	68 851	2.15	498 162	1.64	0.120 2
		3#	2.22	65 299	2.20	502 351	1.58	0.115 6
	10	1#	2.35	146 281	2.33	998 146	1.78	0.100 9
		2#	2.40	165 232	2.48	8 545 642	1.68	0.098 9
		3#	2.44	156 234	2.44	1 082 646	1.74	0.100 8
	15	1#	2.81	129 549	2.82	1 475 992	1.85	0.081 6
		2#	2.72	102 532	2.73	2 019 580	1.82	0.079 8
		3#	2.85	122 321	2.89	1 589 542	1.84	0.082 6
	20	1#	2.92	130 692	2.92	2 296 213	2.45	0.068 0
		2#	3.05	162 642	3.02	2 562 033	2.01	0.067 5
		3#	2.96	205 662	3.00	3 032 320	1.98	0.069 2

5   Conclusions

In this paper, the shear tests have been carried out on intact and discontinuous jointed granite under different normal stresses, and the shear failure mechanism of jointed rock mass has been revealed from the aspects of macro mechanical properties, and acoustic emission characteristics, and mesoscopic evolution law of particle flow. The following conclusions are obtained:

(1) The existence of joints will reduce the shear stiffness and shear strength of rock, and increase the peak shear displacement. Under the combined action of compression and shear, the discontinuous jointed granite cracks mainly propagate along the primary joints and both ends of the rock bridge, forming continuous shear cracks and a certain number of vertical tensile cracks accompanied. With the increase of normal stress, the propagation of secondary cracks is greatly restrained, the total number of cracks tends to decrease, and the specimen changes from tension shear composite failure to shear failure mode.

(2) The characteristics of acoustic emission signals and their key information points are used to effectively predict the shear instability failure of the granite. When the acoustic emission ring counting rate and energy are kept at a low level, the acoustic emission b value is in a high-value state, and the rock is in the initial stage of shear loading or linear elastic deformation. With the acoustic emission signal entering the slow growth stage, the b value will almost synchronously decrease continuously, and the rock will produce an unstable fracture and enter the subcritical instability state, which can be used as an effective precursor of rock shear failure. When the cumulative ringing and energy increase abruptly, the b value will drop abruptly, and the granite specimen will break instantaneously.

(3) The normal stress and joints significantly affect the key points of AE signals. With the increase of normal stress, the acoustic emission ringing count, energy, and the characteristic points of the b value are delayed. When the rock specimen changes from the subcritical instability state to the instability state, the instantaneous released energy increases significantly and the failure is more severe. The existence of joints will reduce the ringing count and energy release value of rock instability, which is consistent with the result that the integrity of rock structure is destroyed by joints and its shear resistance and energy storage capacity are reduced.

References

[1] CHEN Guo-qing, TANG Peng, LI Guang-ming, et al. Analysis of acoustic emission frequency spectrum characteristics and main fracture precursor of rock bridge in direct shear test[J]. Rock and Soil Mechanics, 2019, 40(5): 1649−1656.

[2] CHEN Guo-qing, CHEN Yi, SUN Xiang, et al. Crack

coalescence and brittle failure characteristics of open rock bridges[J]. Chinese Journal of Geotechnical Engineering, 2020, 42(5): 908−915.

[3] ZHOU X P, NIU Y, ZHANG J Z, et al. Experimental study on effects of freeze-thaw fatigue damage on the cracking behaviors of sandstone containing two unparallel fissures[J]. Fatigue & Fracture of Engineering Materials & Structures, 2019, 42(6): 1322−1340.

[4] LIU Shun-gui, LIU Hai-ning, WANG Si-jing, et al. Direct shear test and PFC^{2D} numerical simulation of intermittent joints[J]. Chinese Journal of Rock Mechanics and Engineering, 2008, 27(9): 1828−1836.

[5] LIU Yuan-ming, XIA Cai-chu, LI Hong-zhe. Development in joints research and its application to rock mass containing discontimous joists[J]. Chinese Journal of Underground Space and Engineering, 2007, 3(4): 682− 687.

[6] LIU Yuan-ming, XIA Cai-chu. Advances in research of rock masses containing discontinuous joints in direct shear test[J]. Rock and Soil Mechanics, 2007, 28(8): 1719−1724.

[7] HU Bo, YANG Zhi-rong, LIU Shun-gui, et al. Direct shear strength behavior of rock mass containing coplanar close discontinuous joints[J]. Journal of Engineering Geology, 2008, 16(3): 327−331.

[8] GEHLE C, KUTTER H K. Breakage and shear behaviour of intermittent rock joints[J]. International Journal of Rock Mechanics and Mining Sciences, 2003, 40(5): 687−700.

[9] ZHANG Guo-feng, CHEN Guo-qing, AO Chang-qi, et al. Direct shear test of rock bridge jointed rock mass with different widths[J]. Railway Engineering, 2015, 11: 89−91, 120.

[10] LAJTAI E Z. Tensile strength and its anisotropy measured by point and line-loading of sandstone[J]. Engineering Geology, 1980, 15(3−4): 163−171.

[11] NIU Y, ZHOU X P, ZHOU L S. Fracture damage prediction in fissured red sandstone under uniaxial compression: acoustic emission *b*-value analysis[J]. Fatigue & Fracture of Engineering Materials & Structures, 2019, 43(1): 175−190.

[12] ZHAO Kui, RAN Shan-hu, ZENG Peng, et al. Effect of moisture content on characteristic stress and acoustic emission characteristics of red sandstone[J]. Rock and Soil Mechanics, 2021, 42(4): 899−908.

[13] MORADIAN Z A, EINSTEIN H H, BALLIVY G. Detection of cracking levels in brittle rocks by parametric analysis of the acoustic emission signals[J]. Rock Mechanics and Rock Engineering, 2016, 49(3): 785−800.

[14] MORADIAN Z A, BALLIVY G, RIVARD P, et al. Evaluating damage during shear tests of rock joints using acoustic emissions[J]. International Journal of Rock Mechanics and Mining Sciences, 2010, 47(4): 590−598.

[15] ZHAO Xing-dong, CHEN Chang-hua, LIU Jian-po, et al. Experimental study on AE activity characteristics of different rock samples[J]. Journal of Northeastern University (Natural Science), 2008, 29(11): 1633−1636.

[16] RUDAJEV V, VILHELM J, LOKAJCEK T. Laboratory studies of acoustic emission prior to uniaxial compressive rock failure[J]. International Journal of Rock Mechanics and Mining Sciences, 2000, 37(4): 699−704.

[17] CAI M, MORIOKA H, KAISER P K, et al. Back-analysis of rock mass strength parameters using AE monitoring data[J]. International Journal of Rock Mechanics and Mining Sciences, 2007, 44(4): 538−549.

[18] XU Jiang, LIU Yi-xin, WU Hui, et al. Research on microscopic failure and acoustic emission characteristics of rock under shear load[J]. Mining Safety & Environmental Protection, 2013, 40(1): 12−16.

[19] CHEN Guo-qing, ZHANG Yan, HUANG Run-qiu, et al. Failure mechanism of rock bridge based on acoustic emission technique[J]. Journal of Sensors, 2015, 2015: 964730.

[20] CHENG Li-chao, XU Jiang, FENG Dan, et al. Analysis of mesoscopic cracking propagation and coalescence mechanisms of rocks subject to shearing[J]. Rock and Soil Mechanics, 2016, 37(3): 655−664.

[21] MORADIAN Z A, BALLIVY G, RIVARD P, et al. Evaluating damage during shear tests of rock joints using acoustic emissions[J]. International Journal of Rock Mechanics and Mining Sciences, 2010, 47(4): 590−598.

[22] WANG Gang. Research about strength properties of granite under true triaxial stress state and prediction of strength based on neural network[D]. Shenyang: Northeastern University, 2015.

[23] MU Kang, YU Jin, LI Hong, et al. Acoustic emission of sandstone with hydro-mechanical coupling and PFC-based modelling of energy dissipation[J]. Rock and Soil Mechanics, 2015, 36(5): 1496−1504.

[24] JIANG De-yi, XIE Kai-nan, WANG Jing-yi, et al. Statistical distribution law of acoustic emission energy and waiting-time of sandstone in critical state[J]. Rock and Soil Mechanics, 2017, 38(Suppl.2): 223−228.

[25] LI Yuan-hui, LIU Jian-po, ZHAO Xing-dong, et al. Study on *b*-value and fractal dimension of acoustic emission during rock failure process[J]. Rock and Soil Mechanics, 2009, 30(9): 2559−2563.

[26] LIU Xi-ling, LIU Zhou, LI Xi-bing, et al. Acoustic emission *b*-values of limestone under uniaxial compression and Brazilian splitting loads[J]. Rock and Soil Mechanics, 2019, 40(Suppl.1): 267−274.